IEEE Access
Multidisciplinary | Rapid Review | Open Access Journal

Received November 7, 2019, accepted December 1, 2019, date of publication December 18, 2019,
date of current version December 30, 2019.

Digital Object Identifier 10.1109/ACCESS.2019.2960544

Experimental Study of Atmospheric Turbulence Detection Using an Orbital Angular Momentum Beam via a Convolutional Neural Network

XIAOLI YIN[1,2], XIAOZHENG CHEN[1,2], HUAN CHANG[1,2], XIAOZHOU CUI[1,2], YUANZHI SU[1,2], YILIN GUO[1,2], YONGJUN WANG[1,2,3], AND XIANGJUN XIN[1,2,3]

[1]School of Electronic Engineering, Beijing University of Posts and Telecommunications, Beijing 100876, China
[2]Beijing Key Laboratory of Space-Ground Interconnection and Convergence, Beijing University of Posts and Telecommunications, Beijing 100876, China
[3]State Key Laboratory of Information Photonics and Optical Communications, Beijing University of Posts and Telecommunications, Beijing 100876, China

Corresponding author: Xiaoli Yin (yinxl@bupt.edu.cn)

This work was supported in part by the National Natural Science Foundation of China under Grant 61575027, and in part by the Natural Science Foundation of Beijing Municipality under Grant 4192041.

ABSTRACT Atmospheric turbulence (AT) tends to impair the performance of free space optical (FSO) communication systems. Detecting AT strength is significant for turbulence effect mitigation, which can appropriately guide the selection of turbulence mitigation techniques and modulation formats. Orbital angular momentum (OAM) beam aberrations received through the turbulence channel are closely related to the turbulence strength. In this paper, we experimentally detect the AT strength using an OAM beam based on a convolutional neural network (CNN). We collect 8 kinds of superposed OAM beam intensity images after 5 levels of turbulence in the laboratory as datasets and test the AT detector performance with respect to the number of pixels, mode number of OAM beams, different AT sets and training set size. The results show that the AT detection accuracy is near 100% for 3 kinds of ATs, and the accuracy remains at approximately 85% for 5 kinds of ATs. In addition, using data augmentation methods or a hybrid dataset can improve the AT detection accuracy. The CNN-based method in this paper can help detect the AT strength in atmospheric channels and provide references for choosing appropriate techniques to mitigate turbulence effects and then enhance the OAM-FSO system performance.

INDEX TERMS Free space optical communication, orbital angular momentum, atmospheric turbulence detection, pattern recognition.

I. INTRODUCTION

In recent years, the study of optical vortex beams carrying orbital angular momentum (OAM) has been a popular topic in the free space optical (FSO) communication field [1]. OAM beams have a particular helical phase term of $\exp(il\phi)$, where the OAM mode l, an infinite integer value, is the number of 2π phase shifts across the beam and ϕ is the azimuthal angle [2]. Beams with distinct OAM states are orthogonal to each other, which considerably improves the capacity of communication systems by OAM encoding or OAM multiplexing [3].

When OAM beams propagate in atmospheric turbulence (AT) channels, the random fluctuations of the refractive index cause intensity scintillation, angle of arrival fluctuation, beam wander, and wave-front distortion, which seriously damage the orthogonality of the beams and degrade the OAM-FSO communication system performance [4]–[7]. Researchers have proposed many turbulence effect mitigation techniques under OAM-based FSO communication links [8]–[12]. If the AT channel condition is known in advance, it is possible to guide the selection of optimal approaches to mitigate the effects of AT. In particular, multiple-input multiple-output (MIMO) equalization or spatial diversity combined with MIMO equalization is used to combat the effects of different ATs [1], [8], [9]. Moreover, for the OAM-FSO communication, advance knowledge of the AT strength can help select an appropriate modulation format, specify OAM modes interval and estimate the transmission quality [13]. Thus, it is vitally important to study AT strength detection to enhance system performance.

The associate editor coordinating the review of this manuscript and approving it for publication was Md. Selim Habib.

There have been many methods developed to detect AT. In airborne weather radars, the Doppler spectrum width (DSW) of a weather target echo has been used to determine AT. The pulse pair processing method calculates the DSW by estimating the correlation function of the adjacent pulse echoes; the fast Fourier transform (FFT) method calculates the DSW according to the second-order moment of the echo power spectrum [14]. In wireless optical communication, the refractive index structure constant C_n^2 is used to characterize the AT strength [7], and the traditional methods for calculating C_n^2 are to measure the scintillation index, variance of the angle of arrival fluctuations and beam wander variance [15]–[17]. These methods above need empirical formulas that are established in advance. The measuring results would be limited by the selection and correctness of the mathematical models.

When OAM beams propagate through the AT channel, the AT information is contained in the intensity images, where different ATs cause diverse wave-front distortion and further deform their appearances [13]. Therefore, it is possible to estimate the turbulence strength according to the distorted intensity images. Liu *et al.* [18] proposed and investigated a convolutional neural network (CNN)-based method to retrieve the turbulent phase from the intensity distributions of Gaussian probe beams for correcting distorted vortex beams. In addition, it is possible to deduce the AT strength from the turbulent phase distribution [19], [20]. Furthermore, due to CNNs' strong ability to find intrinsic features with little manual operation [21], pattern recognition based on a CNN can directly detect the AT strength by employing superposed OAM beams [13], which is not bound by empirical formulas or parameterized models. Meanwhile, because OAM beams with different mode numbers have a unique spatial distribution and sensitivity to turbulence, utilizing multiple OAM beams for AT detection increases the diversity of datasets in CNN and has the potential to improve the detection accuracy.

In this paper, we experimentally study AT detection using a CNN for OAM-FSO communication. In Section 2, we introduce the structure of the OAM-based AT detection system, including AT emulation and the CNN architecture. Additionally, we describe our laboratory experimental setup and sample collection. In Section 3, we provide some results about the influence of the number of pixels, mode number of OAM beams, different AT sets and training set size on AT detection accuracy. Finally, in Section 4, we summarize the results of our analysis. The experimental results show that the approach can effectively detect the turbulence strength in atmospheric channels.

II. CONCEPT AND PRINCIPLE

A. OAM-BASED AT DETECTION SYSTEM VIA CNN

A conceptual diagram of the AT detection system based on a CNN is shown in Fig. 1. At the transmitter, the spatial light modulator (SLM), loaded with a series of phase holograms, accordingly modulates the Gaussian beam from the laser into OAM beams. Then, OAM beams propagate through the turbulence channel. At the receiver, a charge-coupled device (CCD) camera is used to capture the OAM beam intensity images, which are input to the CNN for AT detection.

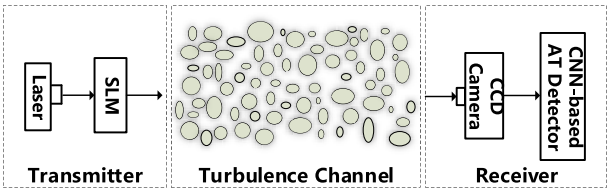

FIGURE 1. Conceptual diagram of the AT detection system based on a CNN. SLM: spatial light modulator, CCD: charge-coupled device.

1) EMULATION OF ATMOSPHERIC TURBULENCE

In this paper, assuming that in a clear weather condition with little attenuation, we emulate the turbulence channel by adding a random phase screen to the beam propagation path. The modified von Karman AT model is adopted, and the spatial power spectrum of the turbulent refractive index fluctuations $\phi_n(\kappa)$ can be expressed as [22]–[25]

$$\phi_n(\kappa) = 0.033 C_n^2 \cdot \exp(-\kappa^2 / \kappa_m) \cdot \left(\kappa^2 + \kappa_0^2\right)^{-11/6} \quad (1)$$

where κ denotes the spatial wavenumber and $\kappa_m = 5.92/l_0$, $\kappa_0 = 2\pi/L_0$, L_0 and l_0 are the outer scale and inner scale of turbulence, respectively, C_n^2 is the refractive index structure constant, representing the turbulence strength.

According to the Markov approximation, the phase spectrum can be written as [22]

$$\phi_\varphi(\kappa) = 2\pi k^2 z \phi_n(\kappa) \quad (2)$$

where k is the wavenumber and z is the propagation distance.

The AT phase screen P can be generated by

$$P = \mathscr{F}^{-1}\left\{\sqrt{\phi_\varphi} C\right\} \quad (3)$$

where $\mathscr{F}^{-1}$ is the inverse 2D Fourier transform and C is a collection of complex Gaussian random variables. To match up with the theory, we add subharmonics to Eq. (3) to compensate low spatial frequencies [23].

In this paper, the refractive index structure constant C_n^2 is set in the range of $1 \times 10^{-16} - 5 \times 10^{-14} \mathrm{m}^{-2/3}$. The turbulence outer scale is 50 m, and the inner scale is 0.02 cm. The simulated turbulent propagation distance is 1000 m, and the number of grid points per side is 512.

2) CONVOLUTIONAL NEURAL NETWORK

The LeNet-5 network, a typical and efficient CNN for handwritten character recognition with a small computational complexity and low memory consumption [26], is selected for tentative AT detection experimental research. Here, the CNN model is used to recognize the AT strength contained in OAM intensity images, and the LeNet-5 network architecture is shown in Fig. 2.

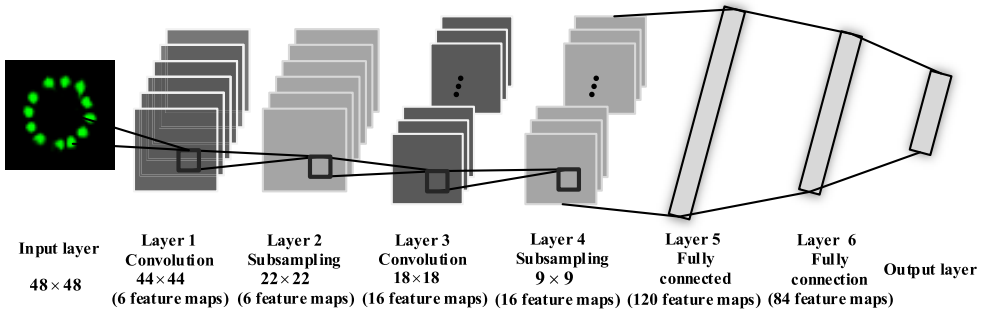

FIGURE 2. Architecture of the LeNet-5 network used as the AT detector.

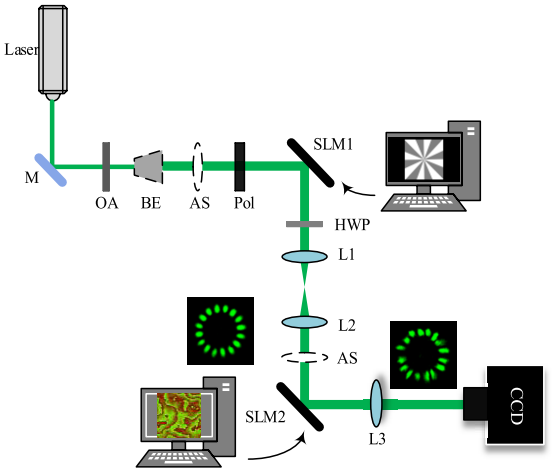

FIGURE 3. Components of the experimental system. M: mirror, OA: optical attenuator, BE: beam expander, AS: aperture stop, Pol: polarizer, HWP: half-wave plate, L: lens.

It should be mentioned that the overfitting problem is caused by an excessive number of network layers or a small amount of training data [27], which can be avoided by using a CNN with a moderate number of layers. Thus, we adopt 8 layers in this paper. Layer 1 in the CNN model is an input layer, and layers 2 and 4 are convolutional layers with 6 and 16 feature maps, respectively, adopting a 5×5 convolutional kernel to extract features. Layers 3 and 5 are subsampling layers with a nonoverlapping 2×2 region for max pooling to reduce the parameters in the network but retain the main features. Layers 6 and 7 are fully connected layers with the tanh function as the activation function, and layer 8 is an output layer to obtain the AT information in OAM intensity images.

The CNN parameter settings are set as follows: the input image is 48 × 48 pixels, the learning rate is 0.1, the size of each mini-batch is 50, and the number of images is 200 per training class and 100 per testing class.

B. EXPERIMENTAL SETUP

A diagram of the experimental setup is presented in Fig. 3. The fundamental Gaussian beam, emitted from a laser with a wavelength of 532 nm, passes through an optical attenuator (OA) and a beam expander (BE), which are used to adjust the beam power and diameter, respectively. The aperture stop (AS) next to the BE is set to filter stray light. As the two reflective SLM1 and SLM2 (Meadowlark Optics, P512-0532-DVI, phase only) are polarization sensitive [28], a polarizer (Pol) is used to convert the Gaussian beam into a linearly polarized beam aligned with the polarization orientation of SLM1. The SLM1, uploaded with different specific phase holograms, is utilized to convert the Gaussian beam to different superposed OAM beams. Similar to Pol, a half-wave plate (HWP) is placed to adjust the OAM beam polarization after SLM1 in alignment with the SLM2 polarization orientation. A pair of lenses is set up for collimation and beam expansion, and the AS next to the lens (L2) is used to filter the extra diffraction orders of OAM beams. The SLM2, uploaded with different turbulence phase holograms, is used to simulate the AT effect on OAM beams. At the receiver, the lens (L3) is placed to allow the far-field intensity to be observed, so as to simulate any propagation distance. Then, the beam is incident to a CCD camera.

TABLE 1. Turbulence types used in the following sections.

AT Types	AT Strength C_n^2 / $m^{-2/3}$
AT_1	1×10^{-16}
AT_2	1×10^{-15}
AT_3	5×10^{-15}
AT_4	1×10^{-14}
AT_5	5×10^{-14}

C. SAMPLE COLLECTION

The distorted OAM beam images captured by the CCD are displayed in Fig. 4. To simplify the expression of turbulence, we list different AT types and the AT strengths in Table 1.

Fig. 4(a) – (e) shows the 8 kinds of superposed OAM beams propagating through the 5 kinds of turbulence $\{AT_1, AT_2, AT_3, AT_4, AT_5\}$, with C_n^2 in the range of $1 \times 10^{-16} - 5 \times 10^{-14} m^{-2/3}$. For each column, with the increase in the level of turbulence, the OAM beam intensity images become

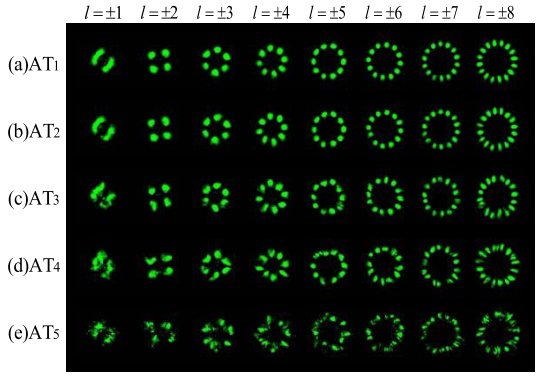

FIGURE 4. Intensity images of different superposed OAM modes $l = \{\pm1, \pm2, \cdots, \pm8\}$ after different turbulence $\{AT_1, AT_2, AT_3, AT_4, AT_5\}$.

TABLE 2. Turbulence sets used in the section.

Sets	AT Types
3ATs	$\{AT_1, AT_3, AT_5\}$
5ATs	$\{AT_1, AT_2, AT_3, AT_4, AT_5\}$

increasingly distorted. Thus, according to the turbulence strength, we can classify the images into 5 categories by row for each OAM beam. Note that we simulate 300 turbulence phase screens for each kind of turbulence strength and randomly load them on SLM2, resulting in 300 different superposed OAM beam intensity images at the receiver for each value of OAM modes $l = \{\pm1, \pm2, \cdots, \pm8\}$.

III. RESULTS AND DISCUSSION

In this section, we combine the five typical turbulence mentioned in Table 1 into two turbulence sets, denoted as 3ATs and 5ATs. As shown in Table 2, the 3ATs set includes AT_1, AT_3, and AT_5, representing weak, medium and strong turbulence, respectively [13], [29]. Then, we remain the 3ATs unchanged, and decrease the turbulence interval by adding two other turbulence to form the 5ATs set, including AT_1, AT_2, AT_3, AT_4, and AT_5.

First, we take the OAM mode of $l = \pm6$ as an example to make a comparison with the AT detection accuracy employing the Gaussian beam ($l = 0$) in the case of 5ATs. In Fig. 5, the testing accuracy versus the number of iterations is shown. When the testing accuracy achieves saturation, the value of $l = \pm6$ is nearly 90%, while the value of $l = 0$ is about 80%. We can see that the AT detection testing accuracy with $l = \pm6$ is higher than that with the Gaussian beam.

In Fig. 6, the training accuracy versus the number of iterations is shown. Here, we display the training process for detecting 5ATs employing OAM modes with $l = \pm1, l = \pm5$ and $l = \pm8$. It can be clearly seen that upon increasing the number of iterations, all the curves escalate and then reach saturation. In addition, the overall training accuracy of the larger mode curves is relatively higher than that of smaller mode curves with the same number of iterations.

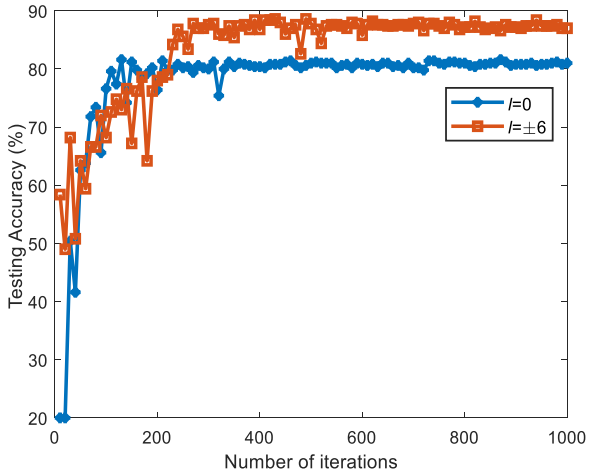

FIGURE 5. The AT detection testing accuracy versus the number of iterations in the case of 5ATs.

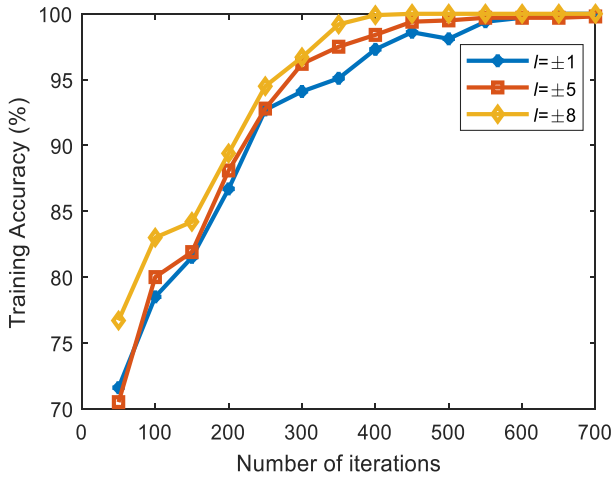

FIGURE 6. Training accuracy versus the number of iterations in the case of 5ATs.

Because the OAM beam with a large mode is more affected by the turbulence [30], the turbulence features contained in the large mode are more obviously distinguishable by the CNN model.

Then, we take the OAM mode of $l = \pm6$ as an example to study the effect of the number of pixels in the input images on the AT detection performance in the case of 5ATs. We show the testing accuracy histogram versus the number of pixels in Fig. 7. It can be clearly seen that the more pixels we set, the higher the accuracy is because the feature details in the input images increase with an increasing number of input pixels [13]. Moreover, we find that when we increase the pixel value to 96×96, the detection accuracy achieves saturation. However, increasing the input image resolution also increases the CNN processing time. We calculate the time consumption for 48×48 pixels as approximately 2.7 times that for 32×32 pixels, while 64×64 pixels consume 4.7 times that of 32×32 pixels and 96×96 pixels consume 10.5 times that of 32×32 pixels. In this paper, considering a trade-off between the detection accuracy and time consumption, we set the image resolution to 48×48. In the case of 48×48 pixels, the CNN

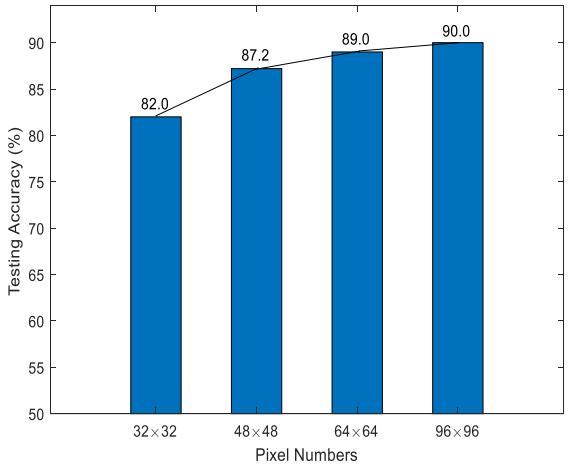

FIGURE 7. The AT detection testing accuracy versus the number of input image pixels, set as 32 × 32, 48 × 48, 64 × 64 and 96 × 96.

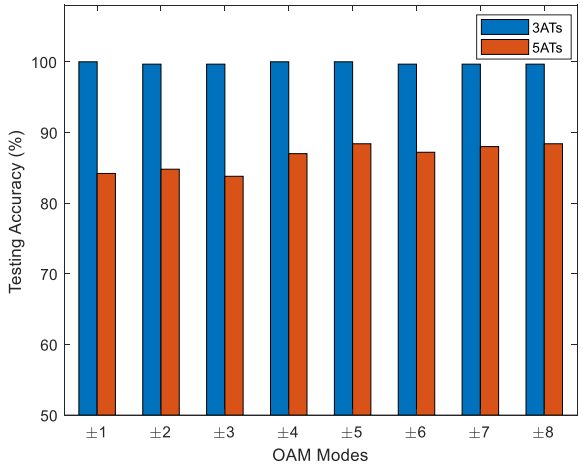

FIGURE 8. The AT detection testing accuracy for OAM modes of $l = \{\pm 1, \pm 2, \cdots, \pm 8\}$ in the cases of 3ATs and 5ATs.

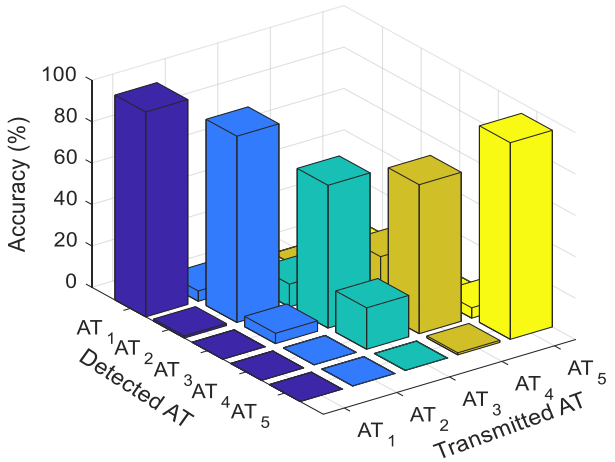

FIGURE 9. The detection testing accuracy and classification error of each AT in the 5ATs set.

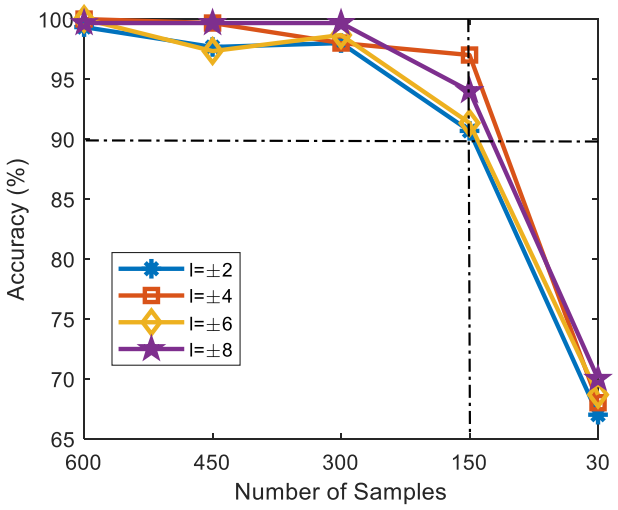

FIGURE 10. Accuracy versus the number of samples in the case of 3ATs with $l = \{\pm 2, \pm 4, \pm 6, \pm 8\}$.

model trained to detect the AT intensity takes approximately 3.4 ms per picture on a personal computer with an Intel Xeon CPU E5-1620 and 32 GB RAM.

Then, we explore the effects of different superposed OAM modes and the interval between ATs on the AT detection testing accuracy. As shown in Fig. 8, the detection accuracy with each OAM mode is almost 100% in the case of 3ATs. Additionally, the accuracy decreases to approximately 85% in the case of 5ATs because when the AT interval decreases, the distortion effect on the OAM modes caused by the AT becomes similar, which increases the difficulty of AT detection. Moreover, the experimental results reveal that the change trend of the AT detection accuracy is not apparent when employing the superposed OAM beam with a mode number from ± 1 to ± 8.

To determine the detection testing accuracy and classification error of each AT in one turbulence set, we take the 5ATs as an example and illustrate the AT detection accuracy histogram versus AT types in Fig. 9. It can be found from Fig. 9 that the detecting accuracies of the weakest AT_1 and strongest AT_5 are approximately 99% and 95%, respectively. Additionally, we find it more likely for adjacent ATs in the intermediate range to misclassify each other.

Next, we study the effect of training set size on AT detection testing accuracy. We reduce the training set size of the 3ATs set from the original 600 samples to 30 samples, but the original test set size of 300 samples remains unchanged. The accuracy curves versus the number of samples are obtained, as shown in Fig. 10. We can see that upon reducing the set size by half, the turbulence detection accuracies of the 4 OAM modes of $l = \{\pm 2, \pm 4, \pm 6, \pm 8\}$ remain above 98%. Then, reducing the size to 150 samples, the accuracies still remain above 90%. Because the training time is related to the training set size, network architecture and computer hardware, an appropriate reduction in the training set size with the same computer hardware and CNN model structure can obtain a lower time consumption.

According to Fig. 10, when reducing the number of samples from 150 to 30, the accuracies decrease appreciably. In the case of the small training set size in Fig. 10, we use

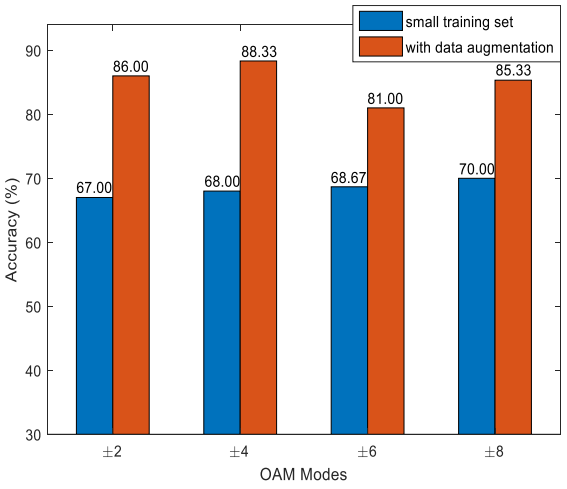

FIGURE 11. Accuracy versus OAM beams of $l = \{\pm2, \pm4, \pm6, \pm8\}$ with or without data augmentation.

TABLE 3. The effect of the hybrid dataset o at detection accuracy.

Set	OAM Modes			
	l=±2	l=±4	l=±6	l=±8
Single dataset	84.80%	87.00%	87.20%	88.40%
Hybrid dataset	85.60%	88.20%	88.60%	90.80%

data augmentation methods, that is, generate more sample data from the existing image samples using rotations and flips, to make the CNN model more robust [31]. We rotate the 30 sample images towards the left or right and flip them horizontally or vertically, creating a new dataset of 150 samples. As displayed in Fig. 11, a better result is produced in which the AT detection accuracy with the 4 OAM modes is greatly improved, from approximately 68% to more than 80%, when we employ data augmentation methods.

Finally, we study the effect of the hybrid dataset on detecting AT in the case of 5ATs. All the datasets, including different OAM modes of $l = \pm2, \pm4, \pm6, \pm8$ (200×5 images per OAM mode), are combined to form a new training set (a total of 4×1000 images), and the single test sets remain unchanged. The results are shown in Table 3, which shows that compared to the single dataset, the accuracy of the model trained with the hybrid dataset is higher. This result is because the hybrid dataset utilizing multiple OAM beams increases the diversity of the intensity images.

IV. CONCLUSION

In this paper, we experimentally demonstrate the CNN-based method employing OAM beams for detecting AT. The results indicate that the higher the number of pixels, the higher the accuracy. The AT detection accuracy in the case of 3ATs is nearly 100% and is approximately 85% in the case of 5ATs. The influence of different OAM modes in our case on AT detection is small, and the large mode has a relatively faster convergence speed than the small mode. We also find that appropriately reducing the training set size can retain a high detection accuracy, and for a small training set size, data augmentation methods can increase the AT detection accuracy. In addition, for the model trained with a hybrid dataset, the AT detection accuracy is higher than for that trained with a single dataset. In future work, we plan to investigate the effects of the OAM mode numbers, the CNN structure and the overfitting problem on the detection performance.

REFERENCES

[1] A. E. Willner, H. Huang, Y. Yan, Y. Ren, N. Ahmed, G. Xie, C. Bao, L. Li, Y. Cao, Z. Zhao, J. Wang, M. P. J. Lavery, M. Tur, S. Ramachandran, A. F. Molisch, N. Ashrafi, and S. Ashrafi, "Optical communications using orbital angular momentum beams," *Adv. Opt. Photon.*, vol. 7, no. 1, pp. 66–106, Mar. 2015.

[2] X. Yin, H. Sang, X. Cui, H. Chang, L. Li, and G. Wu, "Offset tolerance of an orbital angular momentum optical communication system with angular deflection," *Opt. Commun.*, vol. 393, pp. 34–39, Jun. 2017.

[3] J. Wang, J. Yang, I. Fazal, N. Ahmed, Y. Yan, H. Huang, Y. Ren, Y. Yue, S. Dolinar, and M. Tur, "Terabit free-space data transmission employing orbital angular momentum multiplexing," *Nature Photon.*, vol. 6, pp. 488–496, Jun. 2012.

[4] C. Paterson, "Atmospheric turbulence and orbital angular momentum of single photons for optical communication," *Phys. Rev. Lett.*, vol. 94, no. 15, Apr. 2005, Art. no. 153901.

[5] J. A. Anguita, M. A. Neifeld, and B. V. Vasic, "Turbulence-induced channel crosstalk in an orbital angular momentum-multiplexed free-space optical link," *Appl. Opt.*, vol. 47, no. 13, pp. 2414–2429, May 2008.

[6] V. P. Aksenov, V. V. Kolosov, and C. E. Pogutsa, "Random wandering of laser beams with orbital angular momentum during propagation through atmospheric turbulence," *Appl. Opt.*, vol. 53, no. 17, pp. 3607–3614, Jun. 2014.

[7] L. Song, X. Ni, Y. Liu, and Z. Liu, "Comparison of refractive index structure constant deduced from angle of arrival fluctuation and scintillation effects," *Acta Optica Sinica*, vol. 35, no. s1, Jul. 2015, Art. no. 101003.

[8] S. Li, S. Chen, C. Gao, A. E. Willner, and J. Wang, "Atmospheric turbulence compensation in orbital angular momentum communications: Advances and perspectives," *Opt. Commun.*, vol. 408, pp. 68–81, Feb. 2018.

[9] Y. Ren, Z. Wang, G. Xie, L. Li, A. J. Willner, Y. Cao, Z. Zhao, Y. Yan, N. Ahmed, N. Ashrafi, S. Ashrafi, R. Bock, M. Tur, and A. E. Willner, "Atmospheric turbulence mitigation in an OAM-based MIMO free-space optical link using spatial diversity combined with MIMO equalization," *Opt. Lett.*, vol. 41, no. 11, pp. 2406–2409, May 2016.

[10] L. Zou, L. Wang, and S. Zhao, "Turbulence mitigation scheme based on spatial diversity in orbital-angular-momentum multiplexed system," *Opt. Commun.*, vol. 400, pp. 123–127, Oct. 2017.

[11] G. Xie, Y. Ren, H. Huang, M. P. J. Lavery, N. Ahmed, Y. Yan, C. Bao, L. Li, Z. Zhao, Y. Cao, M. Willner, M. Tur, S. J. Dolinar, R. W. Boyd, J. H. Shapiro, and A. E. Willner, "Phase correction for a distorted orbital angular momentum beam using a Zernike polynomials-based stochastic-parallel-gradient-descent algorithm," *Opt. Lett.*, vol. 40, no. 7, pp. 1197–1200, Mar. 2015.

[12] H. Chang, X. Yin, X. Cui, Z. Zhang, J. Ma, G. Wu, L. Zhang, and X. Xin, "Adaptive optics compensation of orbital angular momentum beams with a modified Gerchberg-Saxton-based phase retrieval algorithm," *Opt. Commun.*, vol. 405, pp. 271–275, Dec. 2017.

[13] J. Li, M. Zhang, D. Wang, S. Wu, and Y. Zhan, "Joint atmospheric turbulence detection and adaptive demodulation technique using the CNN for the OAM-FSO communication," *Opt. Express*, vol. 26, no. 8, pp. 10494–10508, Apr. 2018.

[14] Q. Zhang, G. Xiao, Y. Lan, and R. Li, "Atmospheric turbulence detection by PCA approach," *Aerosp. Syst.*, vol. 2, no. 1, pp. 15–20, Aug. 2018.

[15] R. Yuan, Z. Zeng, L. Xiao, C. Ma, N. Weng, and X. Wu, "Comparison of some methods of measuring refractive index structure parameter," *Acta Optica Sinica*, vol. 20, no. 6, pp. 755–761, Jun. 2000.

[16] Y. Gu and G. Gbur, "Measurement of atmospheric turbulence strength by vortex beam," *Opt. Commun.*, vol. 283, pp. 1209–1212, Apr. 2010.

[17] X. Ma, W. Zhu, and R. Rao, "Comparison of refractive index structure constants of atmospheric turbulence deduced from scintillation and beam wander effects," *High Power Laser Particle Beams*, vol. 19, pp. 538–542, Apr. 2007.
[18] J. Liu, P. Wang, X. Zhang, Y. He, X. Zhou, H. Ye, Y. Li, S. Xu, S. Chen, and D. Fan, "Deep learning based turbulence compensation for orbital angular momentum beam distortion and communication," *Opt. Express*, vol. 27, no. 12, pp. 16671–16688, May 2019.
[19] F. Shen and W. Jiang, "Effects of a finite outer scale on the measurement of atmospheric-turbulence statistics with a Hartmann wave-front sensor," *Appl. Opt.*, vol. 41, no. 17, pp. 3385–3391, Jun. 2002.
[20] T. W. Nicholls, G. D. Boreman, and J. C. Dainty, "Use of a Shack-Hartmann wave-front sensor to measure deviations from a Kolmogorov phase spectrum," *Opt. Lett.*, vol. 20, no. 24, pp. 2460–2462, Dec. 1995.
[21] Y. LeCun, Y. Bengio, and G. Hinton, "Deep learning," *Nature*, vol. 521, pp. 436–444, May 2015.
[22] S. Fu and C. Gao, "Influences of atmospheric turbulence effects on the orbital angular momentum spectra of vortex beams," *Photon. Res.*, vol. 4, no. 5, pp. B1–B4, Jul. 2016.
[23] J. D. Schmidt, *Numerical Simulation of Optical Wave Propagation With Examples in MATLAB*. Bellingham, WA, USA: SPIE, 2010.
[24] X. Yin, H. Chang, X. Cui, J. Ma, Y. Wang, G. Wu, L. Zhang, and X. Xin, "Adaptive turbulence compensation with a hybrid input-output algorithm in orbital angular momentum-based free-space optical communication," *Appl. Opt.*, vol. 57, no. 26, pp. 7644–7650, Sep. 2018.
[25] L. C. Andrews, "An analytical model for the refractive index power spectrum and its application to optical scintillations in the atmosphere," *J. Mod. Opt.*, vol. 39, no. 9, pp. 1849–1853, Apr. 1992.
[26] Y. LeCun, L. Bottou, Y. Bengio, and P. Haffner, "Gradient-based learning applied to document recognition," *Proc. IEEE*, vol. 86, no. 11, pp. 2278–2324, Nov. 1998.
[27] Z. Wang, M. I. Dedo, K. Guo, K. Zhou, F. Shen, Y. Sun, S. Liu, and Z. Guo, "Efficient recognition of the propagated orbital angular momentum modes in turbulences with the convolutional neural network," *IEEE Photon J.*, vol. 11, no. 3, Jun. 2019, Art. no. 7903614.
[28] Y. Ren, G. Xie, H. Huang, C. Bao, Y. Yan, N. Ahmed, M. P. J. Lavery, B. I. Erkmen, S. Dolinar, M. Tur, M. A. Neifeld, M. J. Padgett, R. W. Boyd, J. H. Shapiro, and A. E. Willner, "Adaptive optics compensation of multiple orbital angular momentum beams propagating through emulated atmospheric turbulence," *Opt. Lett.*, vol. 39, no. 10, pp. 2845–2848, May 2014.
[29] X. Cui, X. Yin, H. Chang, Z. Zhang, Y. Wang, and G. Wu, "A new method of calculating the orbital angular momentum spectra of Laguerre–Gaussian beams in channels with atmospheric turbulence," *Chin. Phys. B*, vol. 26, no. 11, pp. 232–238, Sep. 2017.
[30] I. B. Djordjevic, J. A. Anguita, and B. Vasic, "Error-correction coded orbital-angular-momentum modulation for FSO channels affected by turbulence," *J. Lightw. Technol.*, vol. 30, no. 17, pp. 2846–2852, Sep. 1, 2012.
[31] T. Doster and A. T. Watnik, "Machine learning approach to OAM beam demultiplexing via convolutional neural networks," *Appl. Opt.*, vol. 56, no. 12, pp. 3386–3396, Apr. 2017.

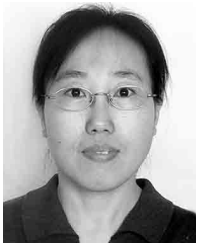

XIAOLI YIN received the B.E. degree in applied electronic technology, the M.S. degree in optics, and the Ph.D. degree in physical electronics from the Beijing University of Posts and Telecommunications (BUPT), Beijing, China, in 1993, 1996, and 2008, respectively. She is currently a Professor at BUPT. Her research interests include optical communication and signal processing.

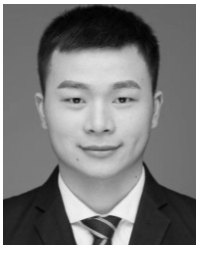

XIAOZHENG CHEN received the B.E. degree from Beijing Forestry University, China, in 2017. He is currently pursuing the master's degree with the School of Electronic Engineering, Beijing University of Posts and Telecommunications. His main research interests include optical communication and adaptive optics.

HUAN CHANG received the B.E. degree from the Beijing University of Posts and Telecommunications (BUPT), China, in 2015, where she is currently pursuing the Ph.D. degree with the School of Electronic Engineering. Her main research interests include optical communication and adaptive optics.

XIAOZHOU CUI received the B.E. degree from the Beijing University of Posts and Telecommunications (BUPT), China, in 2015, where he is currently pursuing the Ph.D. degree with the School of Electronic Engineering. His main research interests include optical communication and machine learning.

YUANZHI SU received the B.E. degree from the Beijing University of Posts and Telecommunications (BUPT), China, in 2018, where he is currently pursuing the master's degree with the School of Electronic Engineering. His main research interests include optical communication and adaptive optics.

YILIN GUO received the B.E. degree from the Beijing University of Chemical Technology, China, in 2016, and the M.E. degree from the Beijing University of Posts and Telecommunications, China, in 2019.

YONGJUN WANG received the Ph.D. degree from Beijing Jiaotong University, Beijing, China, in 2009. He is currently an Assistant Professor with the Beijing University of Posts and Telecommunications, Beijing. His researches focus on high-speed fiber communication systems, including linear and nonlinear compensation in fibers, and recovery of optical signal distortions.

XIANGJUN XIN received the Ph.D. degree from the School of Electric Engineering, Beijing University of Posts and Telecommunications (BUPT), Beijing, China, in 2004. He is currently a Professor with the School of Electric Engineering, BUPT. He is a member of the State Key Laboratory of Information Photonics and Optical Communications, BUPT. His main research interests include broadband optical transmission technologies, optical sensor, and all-optical networks.